Automated Body Contour Detection in SPECT: Effects on Quantitative Studies

Minoru Hosoba*, Hidenobu Wani, Hinako Toyama, Hajime Murata, and Eiichi Tanaka

Medical Systems Division, Shimadzu Corporation, Kyoto; Tokyo Metropolitan Geriatric Hospital, Tokyo; Toranomon Hospital, Tokyo; and National Institute of Radiological Sciences, Chiba, Japan

To perform accurate in vivo quantitation by single photon emission computed tomography, we have developed a new method for detecting body contours for the correction of tissue attenuation. Our method can rapidly derive the best fit contours throughout the body by using the measured axial length of the patient body and Fourier filtering the detected contours which are defined by a unique bit-plane algorithm. We have also evaluated the effects of the body contours on the reconstructed images by using various attenuation correction techniques including a precorrection method (Sorenson, 1974), a postcorrection method (Chang, 1978), a weighted backprojection method, and a radial post correction method (Tanaka, 1983 and 1984). Counts in the specified region-of-interest in phantom images reconstructed by the radial postcorrection, weighted backprojection, and postcorrection methods were more strongly affected by inaccurately detected contours than were counts derived from images reconstructed by the precorrection method.

J Nucl Med 27:1184–1191, 1986

Single photon emission computed tomography (SPECT) with a rotating gamma camera system (*1,2*) or with a ring-detector system (*3*) has progressed remarkably in the recent years, as new radionuclides, such as iodine-123 iodoamphetamine ([^{123}I]IMP) have accelerated the utilization of SPECT in routine clinical studies (*4*). Efforts directed towards quantification of SPECT data have been expected, however, various factors make quantification of SPECT difficult (*5*). These include (a) limited spatial resolution, (b) nonuniformity of the detector, (c) shift in the rotating center of the detector, (d) photon absorption, (e) scattering, and (f) statistical noise. Among these, photon absorption is one of the major problems which has not been completely overcome, although the attenuation correction methods by Sorenson (*6*) and Chang (*7*) have been useful (*8*). Tanaka developed the generalized weighted backprojection method (WBP) (*9,10*), and Tanaka et al. (*11*) presented the simplified version of WBP called radial post correction (RPC). These methods have provided accurate attenuation correction in a uniform attenuator (*10*). The more accurately the attenuation correction can be performed, the greater the need for an accurate determination of the body contour. Various methods for obtaining the body contours have been reported (*1, 12–15*) and reviewed by Gullberg et al. (*16*). These methods use the photopeak data (*14,15*), the Compton scattered data (*1*), the transmission data (*12,13*), or data from the ring source placed around the body (*16*). From the practical point of view, the method using the transmission data or ring source requires additional data acquisition which increases the study time, subjecting the patient to prolonged immobility, and cannot be thought as being feasible for routine clinical work. Although the methods which use photopeak window or Compton window can only redetermine convex contours, they seem to be simpler and more practical in routine SPECT studies.

We have developed a rapid and accurate method to detect the body surface contours using only the photopeak window data and have applied it to clinical studies. We have also investigated the influence of the detected contour on the reconstructed images with the various absorption correction techniques.

Received June 18, 1985; revision accepted Dec. 31, 1985.

For reprints contact: Minoru Hosoba, MS, Medical Systems Division, Shimadzu Corp., 1 Nishinokyo-Kuwabaracho, Nakagyo-ku, Kyoto 604, Japan.

*Present address: Medical Systems Division, Shimadzu Corp., 1 Nishinokyo-Kuwabaracho, Nakagyo-ku, Kyoto 604, Japan.

MATERIALS AND METHODS

SPECT System

The SPECT system employed was equipped with a rotating gamma camera* interfaced to a nuclear medicine computer.† The data were acquired with a 64 × 64 matrix in 64 views covering over 360° or in 32 views over 180° (for the thallium-201 (^{201}Tl) myocardial SPECT scan) using a high-resolution, parallel hole collimator and a circular orbit of 20-cm radius. The linear sampling interval and slice thickness were ~6mm each.

Method for Detecting Body Contours

Figure 1 shows the procedure for detecting the body contours. The total counts of the sinogram are calculated and averaged by the number of pixels with values greater than zero. The threshold levels are then defined as specified percentages of the maximum average counts over all the sinograms. Projection data in the sinogram are smoothed twice using the weighted three-point average method with weighting factors of 1, 2, and 1, respectively. Starting from the point to which the center of rotation is projected (usually #32 of 64 points), the points across the threshold levels are searched in both directions (#32 to #1 and #32 to #64). The point of the edges thus defined in the 64 projections are backprojected onto the bit pattern array consisting of 64 × 64 pixels each with the value of zero or one (Fig. 1A). Figure 1A is backprojected for each of the two edges for each profile. This procedure can only be done by drawing the straight lines on the bit array, so it is performed much faster than in the ordinary back-projection method. When all the edges on the projection are backprojected, an area shaped like a "lake" appears at the center surrounded by tangential lines with a value of 1 (Fig. 1B). In Fig. 1C, which is a magnified illustration of Fig. 1B, the hatched pixels have values of 1 while the others have zero values.

First, from the center of the "lake", a "shore" that is the border of the "lake" is searched out. In the example shown in Fig. 1, pixel ① is found as the "shore". Starting from the pixel ①, a next "shore" pixel is searched using a unique border tracer. The tracer consists of 3 pixels × 3 pixels and places the "shore" pixel previously found at its center (Fig. 1D). The tracer checks the surrounding

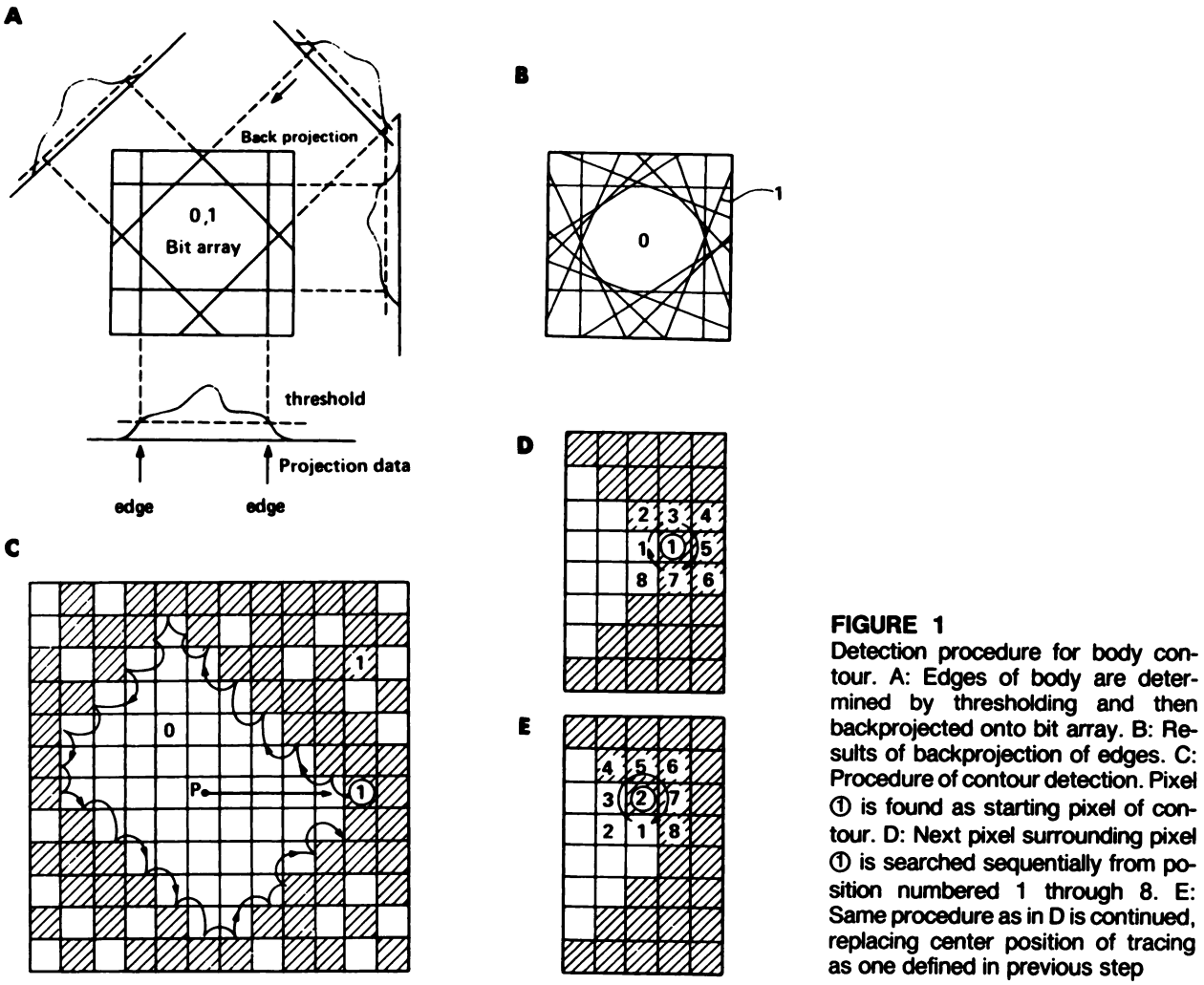

FIGURE 1
Detection procedure for body contour. A: Edges of body are determined by thresholding and then backprojected onto bit array. B: Results of backprojection of edges. C: Procedure of contour detection. Pixel ① is found as starting pixel of contour. D: Next pixel surrounding pixel ① is searched sequentially from position numbered 1 through 8. E: Same procedure as in D is continued, replacing center position of tracing as one defined in previous step

eight pixels clockwise, starting from the position number 1 in Fig. 1D and finds the pixel numbered 2 as the next "shore". The tracer then changes its center pixel to the pixel numbered 2 (Fig. 1D) and starts searching for the next "shore" from the position numbered 1 in Fig. 1E. Starting position is selected not to include the "shore" pixel which had already been found. The starting position can be uniquely defined from knowledge of the position previously found. This procedure is continued until the tracer meets the same pixel which was found in the first step (Fig. 1C).

The body contour thus obtained is fitted with a fourth-order Fourier series in the polar coordinates and then transferred back to the orthogonal coordinates. The fourth-order Fourier series used here is expressed by

$$R(i) = \frac{ao}{2} + \sum_{j=1}^{4} (a_j \, COS(2\pi ij/N) + b_j \, SIN(2\pi ij/N)), \quad (1)$$

where N is the number of radial lines (N = 64), i is the line number, R(i) is the length of a radial line i, j is the harmonic number, and the a_j, b_j are the coefficients of the cosine and sine, respectively. The purpose for fitting the detected points of the body contour to the Fourier series is to reduce the noise of the contour and also to remove the aliasing artifacts which appear in the correction procedure for attenuation.

As a next step, when the body contour fitted with the Fourier series is obtained at the selected threshold level, the algorithm compares the length of the major axis of the detected contour with that measured from the patient. If a discrepancy between these contour sizes is found, the threshold level is then changed, depending on the direction to be adjusted, and the contour searching procedure is started again. When the discrepancy becomes <1%, this procedure is stopped and the final contour is obtained. The threshold level thus defined is used for the contour detection of all slices. This entire procedure is illustrated in Fig. 2.

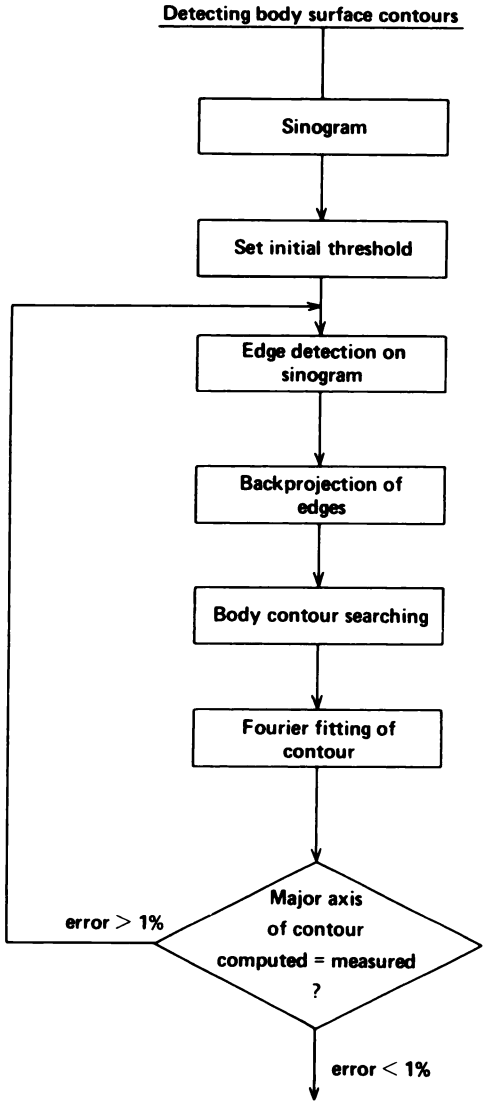

FIGURE 2
Procedure for optimizing detected contours using measured width of body is shown in flowchart

Comparison of Various Attenuation Correction Methods

The weighted backprojection method (WBP) (*9*), radial postcorrection method (RPC) (*11*), the precorrection method by Sorenson (*6*), and the postcorrection method by Chang (*7*) were programmed and installed in the nuclear medicine computer system† (a 16-bit CPU with 256K bytes of memory and floating point processing units) using FORTRAN. The methods used for comparison are described elsewhere (*11*). The same body contours, obtained by the newly developed method described above, were used to reconstruct images using the various attenuation correction methods. A Shepp and Logan (*17*) convolution kernel was used for reconstruction and a value of 0.15/cm was used for the attenuation coefficient for technetium-99m (^{99m}Tc).

Two-dimensional Butterworth filters with cutoff frequencies between 0.4 and 0.6 cycles/cm were used before reconstruction (*18*). These two-dimensional filters can provide isotropic point response in SPECT images (*18,19*), and consequently, the smoothly continued body contours can be obtained in the direction of the body axis.

Phantoms and Patients

A phantom consisting of a simulated liver filled with ^{99m}Tc with three spherical defects was placed inside the Alderson body phantom filled with ^{99m}Tc as background activity. To evaluate the accuracy of the detected contours, this phantom was scanned with relatively high background activity, 35% of the target concentration.

To compare the influence of the detected contours on the reconstructed images using various attenuation correction methods, a 20 cm long cyclindrical phantom with an internal diameter of 20 cm containing a 5 cm diameter plastic sphere filled with ^{99m}Tc was imaged. The center of the plastic sphere is placed 5 cm from the center of the phantom. The surrounding background activity in the phantom is set to ~25% of the radionuclide concentration in the sphere. Another phantom, 30 cm in diameter and 20 cm long, filled with ^{99m}Tc and containing a "cold spot" rod of 5 cm diameter placed at the center was also imaged. A total of 200k counts was acquired for a slice used for comparison of various attenuation correction methods.

Patient data for various organs such as the brain, cardiac pool, myocardium, liver, and kidney were acquired using [^{123}I]IMP, [^{99m}Tc]RBC, ^{201}Tl, [^{99m}Tc]phytate, and [^{99m}Tc]DMSA, respectively.

The projection data were corrected for nonuniformity with a 30 million counts ^{99m}Tc flood. Compensation for the scattered photons was not performed.

RESULTS

The accuracy of the resultant contour obtained by the new method was evaluated by an experiment using the Alderson body phantom. Evaluation was performed using %ERROR which is defined as

$$\%\text{ERROR} = \sum_{i=1}^{N} \frac{|\text{Li} - \text{li}|}{\text{Li}} \cdot 100, \qquad (2)$$

where Li is the true length of the ith radial line, li is the length of the ith radial line of a detected contour and N is the total number of radial lines (N = 64) (Fig. 3A). The contours obtained by the thresholding algorithm from the reconstructed images without attenuation correction were compared with the actual phantom shape in the specified slices and good agreement with maximum deviation of 6 mm was found. In Fig. 3B, an example of the detected contour (C) is plotted superimposing with the true contour (T). The contour first found on the bit array consisting of 64 by 64 matrices was plotted in Fig. 3C. It was fitted with the fourth-order Fourier series in the polar coordinate. The sequentially obtained contours throughout a phantom are displayed in a perspective view (20 slices with 0.6-cm intervals). They were obtained in the analytic form, that is the fourth-order Fourier series, to prevent the higher frequency noise appearing in the reconstruction stage.

Stable contours were delineated with this new method and a calculated %ERROR in this phantom study was 2.0% for 20 slices. In Fig. 4, the detected contours are shown superimposed with the reconstructed images by the RPC method. A total of 700k counts was acquired for the slice reconstructed in Figs. 3 and 4. Another experiment using the Alderson body phantom was performed with lower background activity (10%) and the same results were obtained.

As the method for detecting contours is based on thresholding, inaccurate threshold level may cause errors in the contour. In Fig. 5A, the detected contours

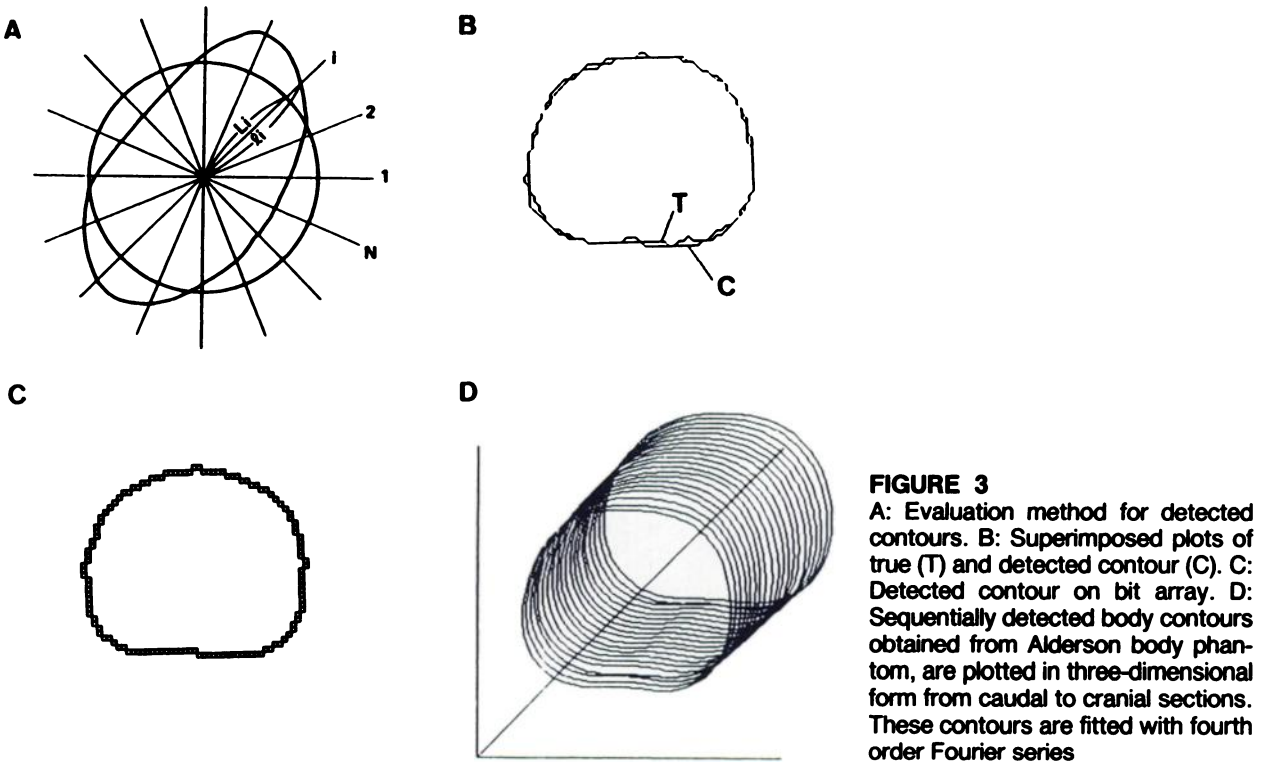

FIGURE 3
A: Evaluation method for detected contours. B: Superimposed plots of true (T) and detected contour (C). C: Detected contour on bit array. D: Sequentially detected body contours obtained from Alderson body phantom, are plotted in three-dimensional form from caudal to cranial sections. These contours are fitted with fourth order Fourier series

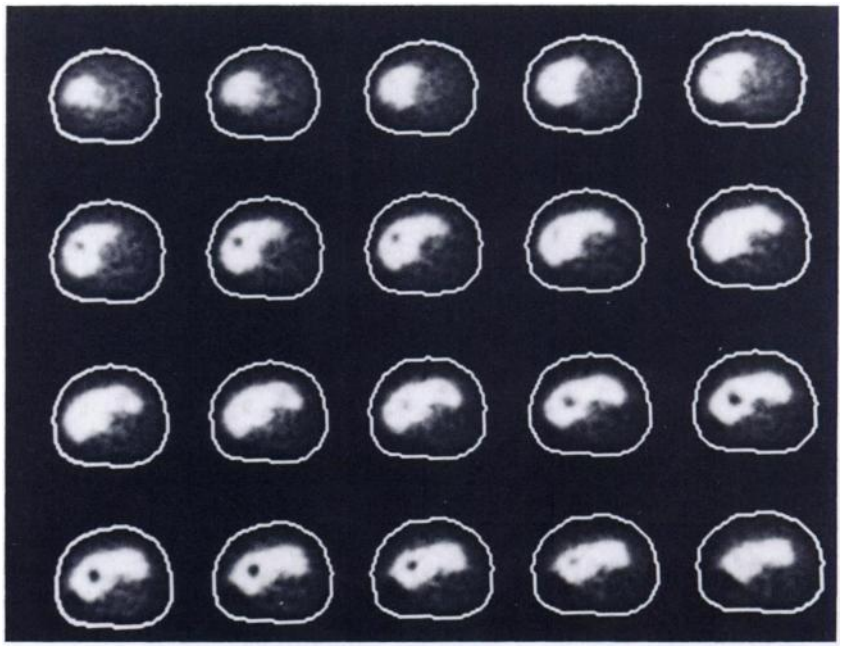

FIGURE 4
Detected contours are superimposed with reconstructed images of liver phantom placed in Alderson body phantom using RPC method

are plotted with various threshold levels ranging from 0 to 100% in steps of 5%, superimposed on the reconstructed image which has been obtained from a cardiac pool image with [^{99m}Tc]RBC. Similar shapes for contours were obtained with the threshold levels ranging from 0 to 40%. The relationships between the threshold levels used for detecting the body contour and the major axial length of the detected contours is plotted in Fig. 5B. The reason why the size of the major axis does not reduce to zero even when the threshold level reaches to 100%, is that the decision concerning the levels was made with the average counts on the sinogram and not with the peak counts. This result demonstrates the difficulty of finding a fixed threshold value. Our method of finding the optimum contour, shown in Fig. 2, which assumes the similarity of the contours within a certain range of threshold levels works well in this case, but it takes several steps to have it converge on the optimal contour (1 sec/step). The computation time can be shortened if the empirically defined threshold level is used as an initial value.

The influence of the detected contour on the density of the reconstructed image with the various attenuation correction methods is shown in Fig. 6 for the case of the 20-cm phantom. Here a slice through the center of the sphere was used. The threshold levels are changed from 5 to 85% in steps of 20%, and the shapes of the detected contours with these thresholds are displayed in Fig. 6A. The region of interest (ROI) is outlined on the image (ROI-A in Fig. 6A). The total counts in ROI-A in the reconstructed images with post, RPC, and pre methods plotted against the major axial length of the detected body contours (Fig. 6B) which deviated from the true values due to changes in the threshold levels.

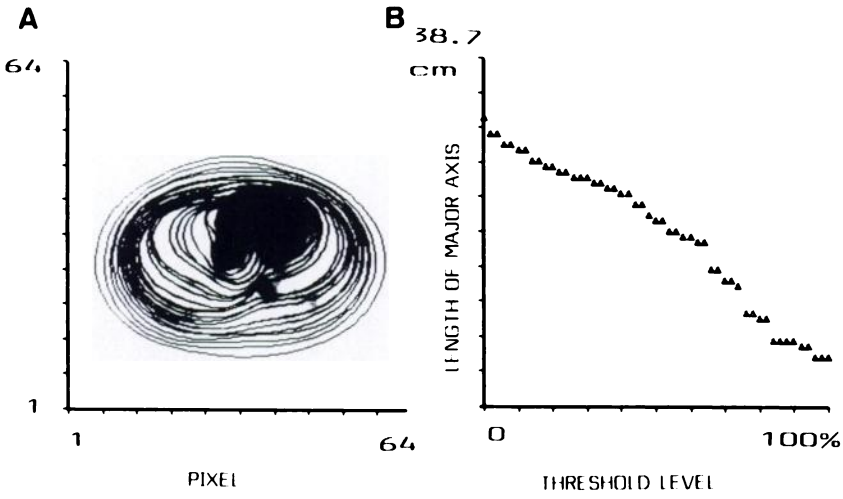

FIGURE 5
A: Detected contours with various threshold levels superimposed on reconstructed image of [^{99m}Tc]blood-pool tomography. B: Relationships between threshold levels and major axial length of contours are plotted

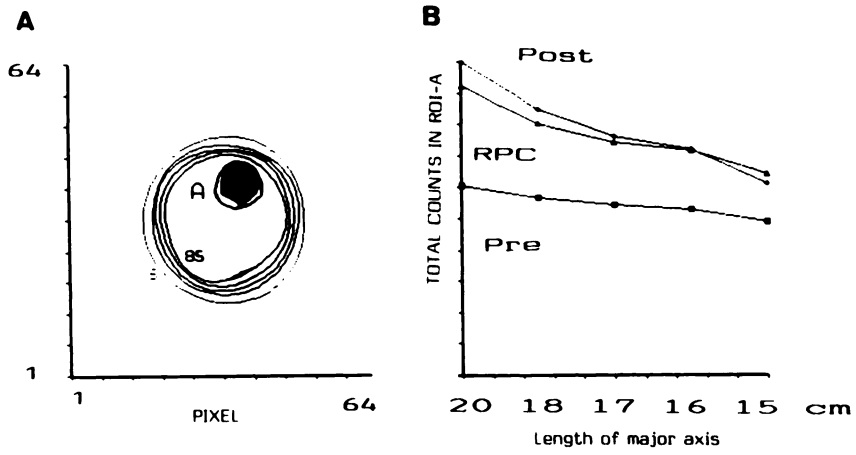

FIGURE 6
Influence of body contours on count density of reconstructed images by three attenuation correction methods: RPC, post, and pre. A: Detected contours of 20-cm water phantom with plastic sphere filled with ^{99m}Tc. Threshold levels are from 5 to 85% in steps of 20%. B: Total counts in ROI-A are plotted against major axial length of detected contour

Total counts at the peak equals 20k counts. Post and RPC methods are strongly affected by the size of the contours. An approximate 1.5 cm change in major axial length (2.3 pixels) of the contour caused 15% in decreased counts in the ROI with the post, 12% with RPC, and 5% with pre method. The reconstructed images of the 30-cm phantom by the various absorption correction methods are displayed in a bird's-eye view in Fig. 7 for investigation of the effects of the error caused by the contour. A total of 200k counts was acquired for the slice reconstructed in Fig. 7. Images in the upper half are reconstructed using inaccurate body contour (32 cm in diameter) and those at the bottom, with accurate contour. Note that the images in the upper half have an "illegal" shoulder at the slope and bulging of the count at the center, which decreases the lesion contrast of the "cold spot".

DISCUSSION

The accuracy of the body contour becomes more important when accurate absorption correction is introduced. Although acquisition of transmission data is most desirable for obtaining perfect body contours, it is necessary to collect the SPECT data twice; and this increases the imaging time for the patient. The use of a reconstructed image of the emission scan may provide arbitrary nonconvex contours, but this is also time consuming. Obtaining the body contour directly from

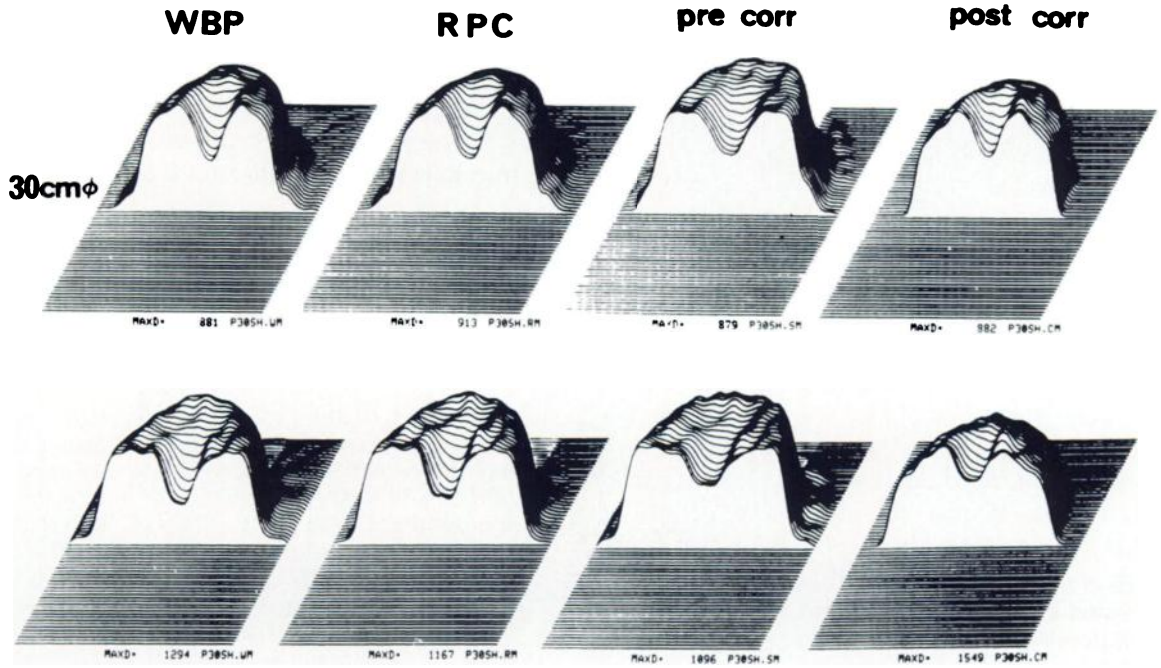

FIGURE 7
Effects of inaccurate body contour on reconstructed image (upper half) with various attenuation correction methods. Images in bottom half are reconstructed with accurate body contour

the projection data is limited to convex contours. However, it is simple, relatively fast and applicable to routine clinical studies.

Jaszczak et al. (*1*) developed an algorithm to use the projection data both from the photopeak and the Compton scatter window. Webb et al. (*15*) applied a technique similar to that of Jaszczak et al. (*1*), using only the photopeak window data. Bergstrom et al. (*14*) introduced the method to obtain body contour for positron emission computed tomography (PET) by finding the edges from the first derivative of the projection data. However, the maximum derivative method itself will cause instability of contours in SPECT studies because of the limited photon events when compared with PET.

Our photopeak method provides results similar to the method of Bergstrom et al. (*14*). The points of differences from the other photopeak methods are as follows. First, arbitrary convex contours are obtained by fitting detected points with the Fourier series. In the method described by Webb et al. (*15*) an ellipse is fitted to the measured points of the body contour. Second, our method performs the entire procedure for detecting body contour on the bit array, and seems much simpler and faster than the other methods. For example, the method of Bergstrom et al. (*14*) takes 30 sec to compute a body contour. Our method can detect a contour within 1 sec. Third, our method can detect the best fit contour using the measured axial length of a patient's body. The characteristics of body contours obtained by our photopeak method using a threshold algorithm (Fig. 5) are similar in shape within a range of threshold levels. Considering these facts we introduced the threshold definition algorithm using measured patient data consisting of the major axial length of the body (Fig. 2). Fourth, two-dimensional Butterworth filtering of the original projection images is performed to get smoother sequential contours throughout the body.

We have shown the method for detecting convex body contours from projection data only. Although the Compton scattered data were not taken into account in our method, they are included in the photo peak window data to some degree (*15,16*). The thresholding methods cannot define the edge points uniquely, yet it is stable in spite of poor counting statistics. In the patient study shown in Fig. 5, the contours deviate significantly according to the threshold levels. It is difficult to use the fixed threshold levels defined empirically (*1,15*) for individual patients, and the optimizing procedure illustrated in Fig. 2 using the length of the major axis of a patient is more effective.

The results shown in Figs. 6 and 7 indicate the importance of obtaining an accurate body contour for establishing quantification for SPECT. The accuracy of the contour was investigated by Bergstrom et al. (*14*) in the PET study comparing it with the x-ray CT, but the detailed experiments for SPECT study were not performed completely. Gullberg et al. (*16*) demonstrated the effect of boundary errors on the reconstructed image caused by the shifted contour, but this may not be the case for an actual patient study. The error is caused mainly by an inaccurate contour size which is shown in Figs. 6 and 7. A more systematic study on the effects of the contour error has been done by Hawman (*21*) with Chang's method (*7*) using computer simulation. However, the estimated error caused by the inaccurate shape of the simulated contour can be eliminated by the Fourier filtering of the contour (*20*). In our method, the order of the Fourier series to filter the contour has been set to four to remove the noise and preserve the shape of the detected contour.

The images by the RPC, WBP, and post methods are severely affected by the detected contour. The comparison between the various absorption correction methods was reported by Tanaka et al. (*11*). The same tendency whereby the sensitivity at the center is lower in the image treated with the pre as compared with RPC, WBP, and post methods is shown in Fig. 7. As it requires much time to compute the correction matrix for arbitrary convex contours for post method, an elliptic contour is being used by most manufacturers (*8*). Care must be taken, however, to ensure that the error caused by the contours will not increase using the simpler approaches, such as fitting to an elliptic contour.

FOOTNOTES

* ZLC-7500: Siemens Gammasonics, Inc., Des Plaines, IL 60018.

† SCINTIPAC-2400: Shimadzu Corp., 1 Nishinokyo-Kuwabaracho, Nakagyo-ku, Kyoto 604, Japan.

ACKNOWLEDGMENTS

The authors thank Noboru Shimizu (Toranomon Hospital) for his kind assistance and discussions in the phantom experiment.

REFERENCES

1. Jaszczak RJ, Chang LT, Stein NA, et al: Whole-body single-photon emission computed tomography using dual large-field-of-view scintillation cameras. *Phys Med Biol* 24:1123–1143, 1979
2. Jaszczak RJ, Coleman RE, Lim CB: SPECT: Single photon emission computed tomography. *IEEE Trans Nucl Sci* NS-27:1137–1153, 1980
3. Hirose Y, Ikeda Y, Higashi Y, et al: A hybrid emission CT-headtom II. *IEEE Trans Nucl Sci* NS-29:520–523
4. Kuhl DE: Quantifying local cerebral blood flow by N-isopropyl-p-[123I] iodomamphetamine (IMP) tomography. *J Nucl Med* 23:196–203, 1982
5. Jaszczak RJ, Coleman RE, Whitehead FR: Physical

factors affecting quantitative measurements using camera-based single photon emission computed tomography (SPECT). *IEEE Trans Nucl Sci* NS-28:69–80, 1981
6. Sorenson JA: Quantitative measurement of radioactivity in vivo by whole-body counting. In *Instrumentation in Nuclear Medicine. Vol. 2*, Hine GJ, Sorenson JA, eds. New York, Academic Press, 1974, pp 311–348
7. Chang LT: A method for attenuation correction in radionuclide computed tomography. *IEEE Trans Nucl Sci* NS-25:638–643, 1978
8. Jaszczak RJ: Industrial corner—Physical characteristics of SPECT systems. *J Comput Assist Tomogr* 6:1205–1215, 1982
9. Tanaka E: Quantitative image reconstruction with weighted backprojection for single photon emission computed tomography. *J Comput Assist Tomogr* 7:692–700, 1983
10. Tanaka E, Toyama H: *A Generalized Weighted Backprojection Algorithm for Single Photon Emission Computed Tomography.* Proceedings of 8th International Conference on Information Processing in Medical Imaging, Brussels, The Hague, Martinus Nijhoff, 1984, pp 185–201
11. Tanaka E, Toyama H, Murayama H: Convolutional image reconstruction for quantitative single photon emission computed tomography. *Phys Med Biol* 29:1489–1500, 1984
12. Huang SC, Carson RE, Phelps ME, et al: Boundary method for attenuation correction in positron computed tomography. *J Nucl Med* 22:627–637, 1981
13. Maeda H, Ito H, Ishii Y, et al: Determination of the pleural edge by gamma ray transmission computed tomography. *J Nucl Med* 22:815–817, 1981
14. Bergstrom M, Litton J, Eriksson L, et al: Determination of object contour from projections for attenuation correction in cranial positron emission tomography. *J Comput Assist Tomogr* 6:365–372, 1982
15. Webb S, Flower MA, Ott RJ, et al: A comparison of attenuation correction methods for quantitative single photon emission computed tomography. *Phys Med Biol* 28: 1045–1056, 1983
16. Gullberg GT, Malko JA, Eisner RL: Boundary determination methods for attenuation correction in single photon emission computed tomography. In *Emission Computed Tomography: Current Trends*, Esser PD, ed. New York, The Society of Nuclear Medicine, 1983, pp 33–53
17. Shepp LA, Logan BF: Fourier reconstruction of a head section. *IEEE Trans Nucl Sci* NS-21:21–43, 1974
18. Wani H, Takahashi S, Hosoba M: Improvement of the reconstructed image of SPECT using 2D filter. *Jpn J Nucl Med* 20:1215–1217, 1983
19. King MA, Schwinger RB, Doherty PW, et al: Two-dimensional filtering of SPECT images using the Metz and Wiener filters. *J Nucl Med* 25:1234–1240, 1984
20. Hosoba M, Wani H, Hiroe M, et al: A fully automated contour detection for gated radionuclide ventriculography with a slant hole collimator. *J Nucl Med* 25:P89, 1984 (abstr)
21. Hawman EG: Impact of body contour data on quantitative SPECT imaging. In *Nuclear Medicine and Biology*, Proceedings of the Third World Congress of Nuclear Medicine and Biology, Vol 1, Raynaud C, ed. Paris, Pergamon Press, 1982, pp 1038–1041